

# Explainable Synthetic Image Detection through Diffusion Timestep Ensembling

**Yixin Wu<sup>\*</sup>, Feiran Zhang<sup>\*</sup>, Tianyuan Shi<sup>\*</sup>, Ruicheng Yin, Zhenghua Wang, Zhenliang Gan, Xiaohua Wang, Changze Lv, Xiaoqing Zheng<sup>†</sup>, Xuanjing Huang**

School of Computer Science, Fudan University, Shanghai, China

Shanghai Key Laboratory of Intelligent Information Processing

{yixinwu23}@fudan.edu.cn {zhengxq, xjhuang}@fudan.edu.cn

## Abstract

Recent advances in diffusion models have enabled the creation of deceptively real images, posing significant security risks when misused. In this study, we empirically show that different timesteps of DDIM inversion reveal varying subtle distinctions between synthetic and real images that are extractable for detection, in the forms of such as Fourier power spectrum high-frequency discrepancies and inter-pixel variance distributions. Based on these observations, we propose a novel synthetic image detection method that directly utilizes features of intermediately noised images by training an ensemble on multiple noised timesteps, circumventing conventional reconstruction-based strategies. To enhance human comprehension, we introduce a metric-grounded explanation generation and refinement module to identify and explain AI-generated flaws. Additionally, we construct the GenHard and GenExplain benchmarks to provide detection samples of greater difficulty and high-quality rationales for fake images. Extensive experiments show that our method achieves state-of-the-art performance with 98.91% and 95.89% detection accuracy on regular and challenging samples respectively, and demonstrates generalizability and robustness. Our code and datasets are available at <https://github.com/Shadowlized/ESIDE>.

## 1. Introduction

With the booming development of diffusion models such as Stable Diffusion [33], DALL-E 3 [1], Midjourney [27] and Flux, the proliferation of artificially generated images has reached unprecedented levels. While users marvel at the stunning quality of these synthetic visuals, a growing conundrum has also risen: distinguishing these creations from genuine photographs has become increasingly difficult, and the risks of malicious use have also skyrocketed. Can pre-

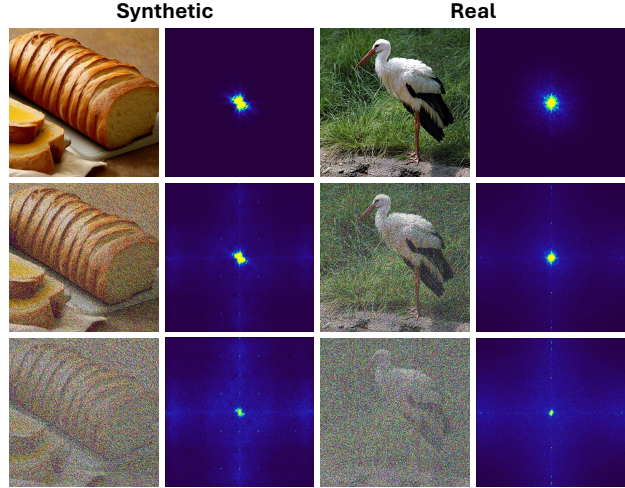


Figure 1. Fourier power spectra of synthetic and real images at timestep 0, 6, 12 of a 24-timestep DDIM inversion process. Artifacts of synthesized images manifest as peaks in the high-frequency components of the spectral background, becoming more pronounced with increasing timesteps.

vailing detection methods keep pace with the sophistication of these knockoffs? Moreover, can current detectors provide explanations robust enough to satisfy skeptics with more than just a feeble yes or no? Existing methods fail to cover more challenging images, and human comprehensibility of detection results is yet to be fully explored. We seek to address these gaps, by improving performance on harder detection samples and integrating high-quality explanations into our pipeline.

Previous studies on synthetic image detection have employed deep neural networks [6, 34, 38, 42], or exploited distinguishable fingerprints in the frequency and spatial domains [5, 8, 19, 49] to determine the fidelity of images. Methods utilizing diffusion-based characteristics such as DIRE, SeDID, LaRE and DRCT [3, 24, 25, 43] focus on detecting discrepancies by reconstructing images through noising and denoising processes, and identifying synthetic

<sup>\*</sup>Equal contribution.

<sup>†</sup>Corresponding Author.

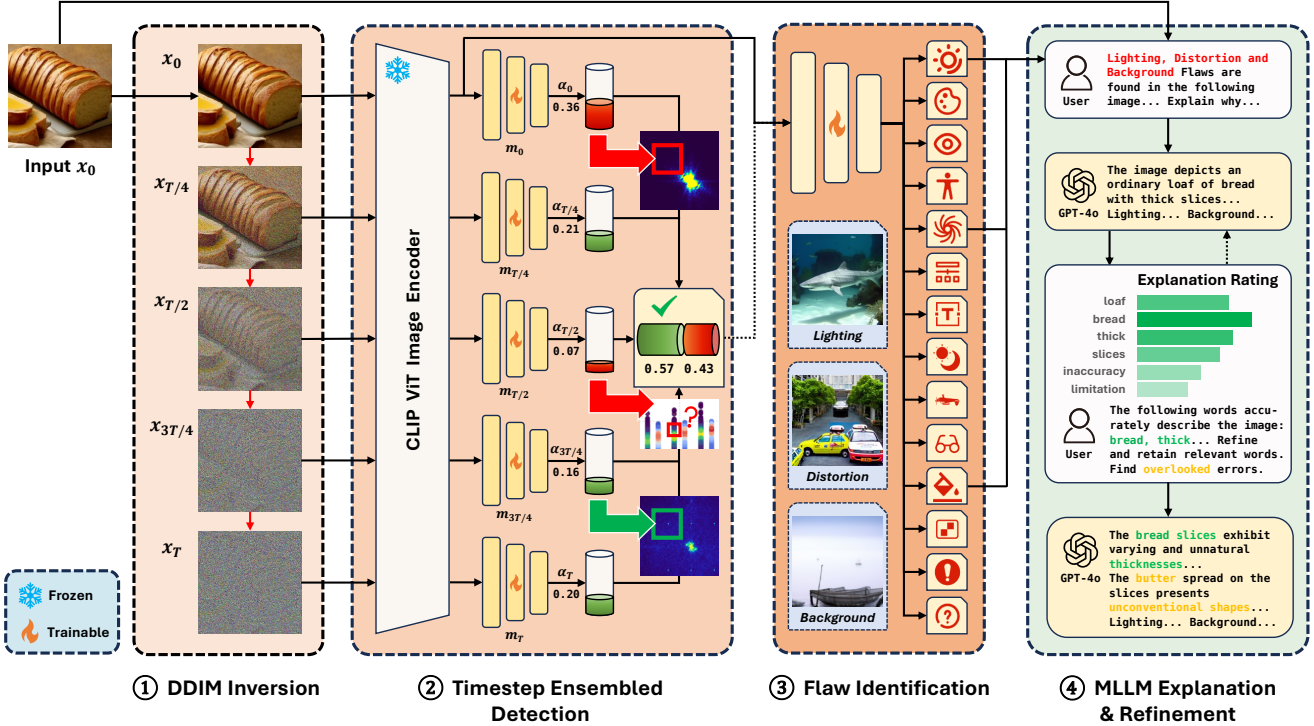


Figure 2. Illustration of the **ESIDE** pipeline. **Stage 1:** DDIM inversion progressively adds noise to input images, creating intermediately noised images. **Stage 2:** Synthetic image detection based on ensembling noised timesteps, discriminators are trained on noised images corresponding to distinct diffusion-induced data distributions, capturing various intermediate features. **Stage 3:** Multi-label flaw identification for synthetic images. **Stage 4:** Explanation generation with MLLMs and rated refinement.

content via reconstruction errors. These works inherently require **both** forward and reverse processes, as their strategies rely on diffusion-based reconstruction.

However, features useful for detection in partially-noised images exist and are often overlooked. As shown in Figure 1, synthetic and real images exhibit distinctions in high-frequency components of their Fourier spectra and manifest differing spectral structures throughout Gaussian diffusion-based noising. Since Fourier transform inherently captures transformation-invariant cues useful for image analysis [31] and is mathematically connected to convolution via the convolution theorem, these frequency-domain features can be

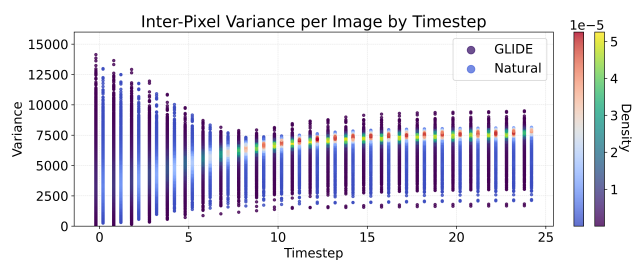
directly extracted. Inspired by [16], we also observe that these images exhibit inconsistent inter-pixel variance distributions across timesteps in terms of spread and peak intensity, depicted in Figure 3. Synthetic and real images demonstrate disparate characteristics at each timestep, providing additional clues possibly usable for detection.

Therefore, we bypass conventional reconstruction measures and propose a pipeline requiring only a **single** noising pass, aiming to directly utilize subtle features within each intermediate noised step, named **ESIDE**: Explainable Synthetic Image Detection through Diffusion Timestep Ensembling, as illustrated in Figure 2. Our framework is designed for detecting generated images of greater challenge and synthesizing high-quality explanations. By circumventing conventional denoising, we halve the time consumed by DDIM [36] pre-processing. Previously under-explored research gaps regarding human comprehension of synthetic images are also addressed, grounding content generated by multimodal large language models (MLLMs) on computable evaluation metrics.

Our main contributions are four-fold:

- We propose a performance-oriented synthetic image detection method based on ensemble learning of diffusion-noised images named **ESIDE**, achieving state-of-the-art

Figure 3. Inter-pixel variances of GLIDE-generated images and natural images noised through DDIM inversion.



performance on both regular and harder samples, while further pushing the limits of detectors to more challenging samples—those that truly demand reliable detection.

- We circumvent conventional image reconstruction measures and provide the insight that varying DDIM inversion intermediate timesteps reveal features directly extractable for detection. To the best of our knowledge, we are the first to systematically explore this approach.
- We introduce an explanation and refinement module into our pipeline for generating precise rationales, bridging the gap of underexplored explainability of generations.
- We construct two datasets: GENHARD and GENEXPLAIN, providing researchers access to images of greater detection difficulty, with synthetic flaws and explanations.

## 2. Related Work

### 2.1. Synthetic Image Detection

Methods that analyze standalone image characteristics without supplementary captions or additional contextual information for synthetic detection could be broadly categorized into three main approaches [14]: deep learning detectors, frequency analysis and spatial analysis.

Deep learning-based detection methods are the most commonly adopted. Early detectors primarily targeted images generated by traditional convolutional neural networks [42]. More recently, methods leveraging vision transformers (ViTs) gained prominence, utilizing CLIP-ViT [30] image encoders for feature extraction, combined with additional classifiers networks or similarity metrics [6, 18, 29, 34, 46]. LGrad used pretrained StyleGAN to convert images into gradients [38]. Other studies that leverage diffusion methods [3, 24, 25, 43] mainly focus on identifying synthetical discrepancies by comparing images with their reconstructions through diffusion noising and denoising.

On the other hand, frequency analysis generally classify synthetic images based on their high-frequency features. Generated images share systematic shortcomings in replicating attributes of high-frequency Fourier modes [5, 8]. Frequency inconsistencies and patterns among images generated with different models could also be effectively utilized for detection [21, 37, 39]. However, utilizing the amplification of distinctions between synthetic and authentic images through intermediate steps of DDIM inversion is yet to be investigated.

Meanwhile, spatial analysis methods detect fake images by computing pixel-level relations and noise patterns. Inter-pixel relationships and contrasts could be captured and used to train detectors [40, 49], while noise patterns of real and synthetic images extracted through spatial models exhibit distinct characteristics usable for classification [4, 19].

### 2.2. Detection Explainability

Previous studies have explored image forgery explanation using MLLMs [12, 13, 47], focusing on identifying manipulations and modifications rather than explaining images synthesized from scratch, lying outside our scope of discussion. Existing synthetic explainers introduce benchmarks rather limited in size, and rely entirely on MLLMs for detection without integrating specialized models and metrics [17, 48]. Latest work [44] utilizes LLaVA [20] for detection, but requires substantial training resources for moderate performance, while the proposed benchmark broadly categorizes based on image content rather than the actual reason it is identified as synthetic.

Instead, our work proposes a light-weighted unified framework combining detection, explanation and automated refinement. We introduce an explanation benchmark for synthetic images named GENEXPLAIN, larger in scale than current benchmarks and categorizing images by their actual synthetical appearance. Manual data pruning revealed a maximal of 67.4% of identified flaws to be incorrect, demonstrating that exclusive reliance on MLLMs proves untrustworthy. By anchoring explanations in classified synthetical errors, and incorporating a refinement process guided by quantitative metrics, we effectively mitigate the limitations of MLLMs in standalone detection tasks.

## 3. Method

### 3.1. Preliminaries

Diffusion models [1, 27, 33] generate images through a two-stage process of forward noise addition and reverse denoising. The forward process gradually transforms data into Gaussian noise, while the reverse trains a neural network to iteratively denoise for distribution restoration. Diffusion models build a symmetric Markov chain connecting the processes, aiming to minimize the KL divergence between data and noise distributions.

The forward process of the Markov chain is defined as:

$$q(x_t|x_{t-1}) = \mathcal{N}\left(x_t; \sqrt{1 - \beta_t}x_{t-1}, \beta_t\mathbf{I}\right), \quad (1)$$

where  $x_t$  represents the noised image at timestep  $t$ , and  $\beta_t \in (0, 1)$  is a predefined noise schedule.

**Denoising Diffusion Probabilistic Models (DDPM)** [35] parameterize the reverse process as a Markov chain:

$$p_\theta(x_{t-1}|x_t) = \mathcal{N}\left(x_{t-1}; \mu_\theta(x_t, t), \sigma_t^2\mathbf{I}\right), \quad (2)$$

where the mean  $\mu_\theta$  is derived from a neural network that predicts the noise  $\epsilon_\theta(x_t, t)$ :

$$\mu_\theta(x_t, t) = \frac{1}{\sqrt{\alpha_t}} \left( x_t - \frac{\beta_t}{\sqrt{1 - \alpha_t}} \epsilon_\theta(x_t, t) \right). \quad (3)$$

**Denoising Diffusion Implicit Models (DDIM)** [36] accelerate sampling by defining a non-Markovian forward process while maintaining the same marginal distribution  $q(x_t|x_0)$ . The reverse process combines deterministic generation with stochastic noise injection:

$$x_{t-1} = \sqrt{\bar{\alpha}_{t-1}} \left( \frac{x_t - \sqrt{1 - \bar{\alpha}_t} \epsilon_\theta(x_t, t)}{\sqrt{\bar{\alpha}_t}} \right) + \sqrt{1 - \bar{\alpha}_{t-1} - \sigma_t^2} \cdot \epsilon_\theta(x_t, t) + \sigma_t \epsilon, \quad (4)$$

### 3.2. Synthetic Image Detection

We propose a novel method for detecting synthetics through ensemble learning of intermediate noise. AdaBoost [9] is a boosting algorithm that aggregates the predictions of multiple weak models through a weighted sum, constructing a stronger learner with enhanced accuracy for discrimination. Specifically, we follow previous ensembling measures, but train classifiers on distinct data distributions, each corresponding to a different diffusion timestep.

Given an input image  $x_0$ , we apply a  $T$ -timestep DDIM inversion process to yield intermediate samples, generating a sequence of stepwise noised images:  $\{x_0, x_1, x_2, \dots, x_T\}$ . For each timestep with an interval of a stride  $s$ , a base classifier  $m_k$  is trained exclusively on corresponding timestep noised images, resulting in a collection of models  $M$ :

$$M = \{m_0, m_s, m_{2s}, \dots, m_T\} \quad (5)$$

A **sample weight**  $w_{k,i}$  is assigned to each image of the training set to emphasize samples previously misclassified, while reducing the significance of correctly predicted cases. As each model operates on a noised dataset corresponding to a different diffusion timestep, the sample weights are separately initialized for each model, where  $N$  represents the total number of images in the training set.

$$w_{k,1} = w_{k,2} = \dots = w_{k,n} = \frac{1}{N} \quad (6)$$

By incorporating  $w_{k,i}$  into binary cross-entropy (BCE), a weighted loss function  $\mathcal{L}_{\text{WBCE}}$  is obtained, where  $y$  denotes the true label and  $\hat{y}$  is the predicted probability:

$$\mathcal{L}_{\text{WBCE}}(k, y, \hat{y}) = \sum_{i=1}^N w_{k,i} [y_i \log(\hat{y}_i) + (1 - y_i) \log(1 - \hat{y}_i)] \quad (7)$$

The weighted error  $\epsilon_k$  of  $m_k$  can then be calculated as follows, where  $h_k(x_i)$  is the prediction of  $m_k$  for  $x_i$ :

$$\epsilon_k = \frac{\sum_{i=1, h_k(x_i) \neq y_i}^N w_{k,i}}{\sum_{i=1}^N w_{k,i}} \quad (8)$$

To form the final prediction, a **model weight**  $\alpha_k$  is assigned to each classifier and updated throughout training:

$$\alpha_k = \frac{1}{2} \ln\left(\frac{1 - \epsilon_k}{\epsilon_k}\right) \quad (9)$$

Sample weights are then adjusted according to the prediction results and normalized across timestep samples:

$$\tilde{w}_{k,i} = w_{k,i} \cdot e^{-\eta \alpha_k \cdot h_k(x_i) y_i} \quad (10)$$

$$w'_{k,i} = \frac{\tilde{w}_{k,i}}{\sum_{i=1}^N \tilde{w}_{k,i}} \quad (11)$$

Here,  $\eta$  is a learning rate factor applied to limit change rate. After training the base classifiers, the model weights  $\alpha_k$  are used to calculate a weighted sum  $H(x_i)$  of the predictions from each  $m_k$  for the final prediction of image  $x_i$ :

$$H(x_i) = \text{sign}\left(\sum_{k=0}^T \alpha_k \cdot h_k(x_i)\right) \quad (12)$$

In practice, a threshold is applied to the weighted error to normalize model weights and prevent degradation.

### 3.3. Multimodal Explanation Refinement

When an image is identified as synthetic, a multi-label classifier is then employed to identify potential flaws present. MLLMs are utilized to generate a rough explanation for each image based on the identified types. An refinement process is iteratively conducted to enhance explanation quality, segmenting the initial explanation into multiple phrases and assigning each a rating based on its semantic similarity with the image. Text-image cross attention [15] mechanisms are leveraged to compute these ratings. Faster R-CNN [32] is first applied for object detection, identifying  $n$  sub-image regions, which are then encoded into visual embeddings  $\{v_1, v_2, \dots, v_n\}$  using a CLIP ViT, while also concatenating the embedding of the full image  $v_0$ . Phrases  $p$  are then encoded into the same vector space, and their similarities with each region are calculated and normalized, pairing these phrases with visual regions. The weighted combination of the region embeddings, denoted as  $a$ , is then derived based on the similarities:

$$\tilde{s}_i = \frac{\cos\langle p, v_i \rangle}{\sum_{i=0}^n \cos\langle p, v_i \rangle} \quad (13)$$

$$a = \sum_{i=0}^n \frac{v_i \cdot e^{\lambda \tilde{s}_i}}{\sum_{i=0}^n e^{\lambda \tilde{s}_i}} \quad (14)$$

where  $\lambda$  denotes the inverse temperature of the softmax function. The **rating**  $r$  of the phrase  $p$  is then calculated as its cosine similarity with  $a$ :

	LI	CS	PS	BA	DO	SC	IT	IS	PV	BB	BG	TX	GF	NE	#		
Midjourney															4,561	Lighting (LI) Color Saturation (CS) Perspective (PS) Bad Anatomy (BA) Distorted Objects (DO) Structural Composition (SC) Incomprehensible Text (IT) Implausible Scenarios (IS) Physical Violations (PV) Blurry Borders (BB) Background (BG) Texture (TX) Generation Failures (GF) Not Evident (NE)	
SD V1.4															7,712		
SD V1.5															4,556		
ADM															6,932		
GLIDE															7,681		
Wukong															7,488		
VQDM															7,822		
BigGAN															7,458		
	#	3,324	510	2,161	13,902	13,651	4,232	4,568	439	1,295	2,811	960	1,908	461	3,988	54,210	

**Flaws:** *Lighting, Distorted Objects, Background*

- The top crust of the bread is *overly bright*, suggesting the presence of *multiple conflicting light sources* rather than a singular direction. The upper layer of butter appears *excessively illuminated* while the lower slice casts an *unrealistic shadow*, lacking alignment with any visible light source. ...
- The slices lack standard uniformity, exhibiting *varying and unnatural thicknesses* that undermine the appearance of a properly sliced loaf. The butter spread on the slices presents *unconventional shapes* and *inconsistent textures*. ...
- The background suffers from *poorly blended monotonous drabness*, dominated by *unvarying brown tones* of the wooden surface. ...

Figure 4. Visualization of the **GenExplain** benchmark. Synthetic images from GenImage are divided into 14 categories of flaws. Each image is matched with one or multiple categories, with a corresponding explanation for each flaw type.

$$r = \cos\langle p, a \rangle \quad (15)$$

For refinement, Top-K sampling is performed according to phrase relevance, and the MLLM is instructed to retain these phrases while identifying additional overlooked flawed regions. This process is iteratively repeated with the revised explanations, resulting in a final explanation that describes the flaws present in the image with greater accuracy.

### 3.4. Construction of GenHard and GenExplain

We construct two datasets, GENHARD and GENEXPLAIN, based on GenImage [50]. The former comprises synthetic and natural images more challenging to detect, while the latter aims to categorize and provide explanations for flaws commonly found in artificial images.

**GenHard** To extract samples of greater difficulty, we employed CBSID [6] with a minimalist linear network classifier under-fittingly trained for a single epoch on the validation subsets of GenImage, and subsequently tested on training subsets. Across the 8 subsets tested, the 108,704 synthetic images and 112,682 natural images misclassified were identified as hard samples, which were then partitioned into training and validation sets.

**GenExplain** Extending prior taxonomies [17, 26, 47], we identified 14 common categories of flaws associated with realistic synthetic images, and constructed a dataset com-

prising 54,210 groups of images, flaws and explanations, illustrated in Figure 4. Images from GenImage validation subsets were fed into `gpt-4o`, prompted with flaw definitions and instructions, yielding a preliminary categorization of approximately 11,000 to 14,000 image-flaw pairs per subset. Manual data pruning removed 30.1% to 67.4% of images incorrectly categorized from each subset, and the final explanations are obtained through iterative refinement.

## 4. Experiments

### 4.1. Synthetic Image Detection

We train an ensemble on groups of noised images derived from DDIM inversion intermediate timesteps, following the implementation provided by [7, 43] and using pre-trained diffusion models of sizes  $256 \times 256$  and  $512 \times 512$ . CLIP ViT-L/14 [30] is employed to extract image features, which are passed through multi-layer perceptrons for classification. After each component model generates a prediction, the final prediction is obtained by computing a weighted sum based on their model weights  $\alpha_k$ .

We evaluate our results on GenImage [50], a million-scale dataset covering 8 generator subsets: Midjourney [27], Stable Diffusion V1.4 [33], Stable Diffusion V1.5 [33], ADM [7], GLIDE [28], Wukong [45], VQDM [10], and BigGAN [2]. Due to computational resource constraints, we partition the validation subsets of GenImage by

Method	Training & Test Subsets								Avg. Acc (%)
	Midjourney	SD V1.4	SD V1.5	ADM	GLIDE	Wukong	VQDM	BigGAN	
ResNet-50	83.90/86.75	80.63/94.17	76.17/90.19	75.81/91.00	<b>95.82</b> /99.00	73.72/89.50	92.94/98.67	<b>99.10</b> /96.08	84.76/93.17
DeiT-S	58.29/76.08	73.92/81.08	74.32/78.75	63.37/68.42	72.84/93.83	71.01/83.83	66.87/77.50	46.23/76.00	65.86/79.44
Swin-T	70.81/91.00	74.63/88.08	78.02/90.00	70.30/79.50	85.19/97.83	74.92/85.92	86.96/90.17	88.24/ <u>99.67</u>	78.63/90.27
CNNSpot	70.91/83.92	78.02/89.25	80.15/88.06	68.32/72.58	78.57/87.08	78.95/87.83	89.97/97.42	70.44/96.08	76.92/87.78
CBSID	67.10/93.25	73.03/90.92	72.22/93.63	94.20/ <u>99.83</u>	88.53/ <u>99.17</u>	75.67/92.75	84.10/98.17	98.27/ <b>99.91</b>	81.64/95.95
DIRE	88.86/92.83	95.72/97.42	96.02/96.25	90.52/94.67	81.40/ <b>99.83</b>	84.17/92.67	94.90/97.83	93.29/ <u>99.67</u>	90.91/96.40
LGrad	72.25/87.33	72.28/83.92	76.45/84.37	70.86/79.17	82.19/96.00	65.50/79.75	74.80/81.08	83.74/94.58	74.76/85.78
UnivFD	40.80/87.75	41.92/89.33	35.40/88.25	65.28/85.58	79.13/94.25	65.35/89.42	67.84/91.92	71.07/94.75	58.35/90.16
FreqNet	87.13/94.33	93.47/94.58	<b>96.73</b> /95.12	95.69/91.50	82.13/98.25	90.88/90.17	<b>98.60</b> /95.42	85.12/99.17	91.22/94.82
NPR	85.10/87.25	89.90/95.25	95.23/97.12	<u>99.36</u> /99.75	86.29/92.08	<b>96.94</b> / <b>98.42</b>	93.74/97.33	92.87/99.58	92.43/95.85
DRCT	<b>92.89</b> /97.50	<b>97.51</b> / <b>100.00</b>	<b>96.10</b> / <b>99.38</b>	88.03/96.67	85.59/98.33	91.29/95.83	96.17/ <b>100.00</b>	97.93/99.17	93.19/ <u>98.36</u>
<b>ESIDE</b>	<u>92.38</u> / <b>98.42</b>	<u>96.65</u> /99.17	<b>96.73</b> /98.63	<b>99.43</b> / <b>100.00</b>	94.98/99.00	91.50/97.25	97.90/99.33	97.58/99.50	<b>95.89</b> / <b>98.91</b>

Table 1. Synthetic image detection accuracy on GenImage subsets. Models are trained individually on each GenImage subset, with the **original** samples training set only, while tested on both the **original** samples test set, and a previously unseen **hard** samples test set from GenHard. The prior number for each cell marks the test accuracy on the **hard** samples, while the posterior marks the test accuracy on the **original** samples. The best scores are highlighted in **bold**, and the second best are underlined.

a 9:1 ratio for training and evaluation.

The baselines ResNet-50 [11], DeiT-S [41], Swin-T [22], CNNSpot [42], CBSID [6], DIRE [43], LGrad [38], UnivFD [29], FreqNet [39], NPR [40], and DRCT [3] (*ICML 2024 Spotlight*) are compared, on both the original GenImage dataset and the more challenging samples curated in GENHARD. Two distinct scenarios are investigated: (1) train-test subsets from the same generator, and (2) train-test subsets sourced from different generators, enabling a comprehensive assessment of performance and generalizability.

**Implementation Details** A total of  $T = 24$  DDIM inversion timesteps are taken. The sample weights learning rate  $\eta$  is set to 0.25, and classifier error thresholds  $\epsilon_k = \min(\max(\tilde{\epsilon}_k, 0.001), 0.5)$  are enforced to prevent model weight overflow and ensemble degradation. We select a stride  $s = 3$  resulting in an ensemble of 9 classifiers, and only require a simple five-layer MLP classifier with an input dimension of 768, hidden layer dimensions of [1024, 512, 256, 128], and a scalar output for such performance, easily adaptable to larger networks. A batch normalization layer, a LeakyReLU activation with a negative slope of 0.1, and a Dropout layer with a dropout rate of 0.5 are sequentially applied after each linear layer. The AdamW optimizer with a learning rate of  $1 \times 10^{-4}$  and weight decay of  $5 \times 10^{-4}$  is employed, alongside our modified weighted binary cross-entropy loss function  $\mathcal{L}_{\text{WBCE}}$ .

Our method is implemented based on PyTorch, exhibits low GPU memory consumption, and enables simple hybrid parallelism as models trained on different noised datasets could easily be allocated to various devices and subsequently combined. Computational support is provided by

NVIDIA L20 48GB GPUs. Training could be further accelerated when image features are precomputed and stored, which sums up as the main overtime.

**Result Analysis** As shown in Table 1, ESIDE achieves SOTA performance on both harder and original images, with an average absolute accuracy increase of at least 2.70% and 0.55% respectively, performing 15.10% better than baseline averages on harder samples and leading by 7.28% on originals. Cross-validation results in Table 2 show generalizability across images synthesized by other models. Notably, some methods perform worse than random guessing on hard samples as only incorrect identifications are included in GENHARD, further underscoring its difficulty. Similar cross-validation results reveal that effective indicators for one generator may perform opposite on another. Since we emphasize training on controversial images, the anomaly of higher cross-validation accuracies on samples of greater difficulty is observed, as original scenarios that should have been simple to classify could be under-trained in comparison.

## 4.2. Error Explanation and Refinement

**Flaw Classification** We propose synthetic flaw detection as a new task, and introduce a simple baseline experimented on GENEXPLAIN. The same classifier architecture as in Section 4.1 is adopted, with output layer dimension adjusted to 14 to match the categories of flaw types. BCE Loss is used, and each label is predicted independently. We partition our dataset by 9:1 for training and evaluation. Evaluation metrics include Exact Match (EM) accuracy and Mean Average Precision (mAP), measuring the proportion of predictions

Method	Test Subsets								Avg. Acc (%)
	Midjourney	SD V1.4	SD V1.5	ADM	GLIDE	Wukong	VQDM	BigGAN	
ResNet-50	45.27/71.17	80.63/94.17	74.06/90.33	<b>75.36</b> /48.17	24.67/57.25	76.91/90.33	49.76/59.75	26.58/41.75	56.66/69.12
DeiT-S	47.88/49.33	73.92/81.08	75.21/79.50	65.21/48.17	25.67/48.92	74.55/80.75	47.89/46.08	31.70/43.58	55.25/59.68
Swin-T	47.14/56.58	74.63/88.08	76.13/86.94	57.71/49.83	21.45/50.33	76.54/84.08	43.24/49.25	26.92/45.08	52.97/63.77
CNNSpot	49.28/56.58	78.02/89.25	78.34/86.19	72.77/48.50	26.36/51.50	74.77/83.42	49.39/50.25	27.13/47.83	57.01/64.19
CBSID	51.16/74.33	73.03/90.92	74.07/91.69	73.69/54.42	49.36/ <b>74.83</b>	73.41/78.33	52.32/ <b>65.58</b>	33.36/59.08	60.05/73.65
DIRE	67.38/62.08	95.72/97.42	95.59/ <b>96.75</b>	49.01/30.50	31.38/17.17	62.18/56.50	33.80/29.25	37.58/19.50	59.08/51.15
LGrad	50.28/56.17	72.28/83.92	73.57/81.92	<b>74.19</b> /44.50	25.05/49.50	55.56/53.83	53.21/52.92	33.46/45.33	54.70/58.51
UnivFD	26.75/ <b>82.42</b>	41.92/89.33	38.66/79.17	61.83/47.08	25.12/71.58	58.17/72.17	54.36/51.58	29.75/49.58	42.07/67.87
FreqNet	<b>68.96</b> /70.50	93.47/94.58	88.52/91.58	67.51/ <b>63.92</b>	48.81/72.58	87.23/78.83	53.61/56.25	<b>70.44</b> / <b>71.83</b>	<b>72.32</b> / <b>75.01</b>
NPR	47.35/53.75	89.90/95.25	96.01/93.50	70.95/ <b>55.42</b>	50.80/65.58	<b>95.53</b> / <b>96.08</b>	58.27/49.33	41.61/46.08	68.80/69.37
DRCT	51.52/46.17	<b>97.51</b> / <b>100.00</b>	<b>97.51</b> /86.50	69.36/53.50	<b>55.68</b> /67.42	86.42/89.50	<b>62.91</b> /56.25	44.39/52.25	70.66/68.95
<b>ESIDE</b>	<b>67.40</b> /74.33	<b>96.65</b> /99.17	<b>97.15</b> / <b>98.75</b>	63.79/37.08	50.21/39.00	82.60/67.33	59.73/50.42	<b>90.10</b> /53.67	<b>75.95</b> /64.97

Table 2. Cross-validation accuracy on GenImage subsets. Models are trained on GenImage/SD V1.4 with the **original** samples training set only, while tested on both the **original** and **hard** samples test set from GenHard.

Metric	MJ	SD1.4	SD1.5	ADM	GLI	WK	VQ	BG	Avg.
EM	41.60	52.03	58.08	50.41	49.72	33.81	54.61	49.07	48.67
mAP	34.70	35.71	33.01	40.04	34.57	33.80	54.05	34.50	37.55

Table 3. Performance of 14-type flaw classification on GenExplain subsets. Subset names are abbreviated.

The AI-generated image exhibits the systematic error of distorted objects, particularly evident in the *sliced bread* and the *buttered portions*. The *slices* of *bread* show an unnatural curvature and uneven thickness, deviating from the expected straight cuts found in *typical loaves*. Additionally, the *butter* appears to be inconsistently spread, with some areas looking excessively thick and others almost non-existent, leading to an unrealistic presentation. These anomalies create an illusion of warped forms, which detracts from the recognizable and expected features of unprocessed bread and butter.  $\text{sim}_5 = (\text{bread} + \text{sliced bread} + \text{unprocessed bread} + \text{butter} + \text{typical loaves}) / 5 = 0.235$

Figure 5. Illustration of phrase-image similarities in an explanation snippet and calculation of Top-5 average.

where all 14 labels are correctly matched, and the mean value of average precisions across all labels. Results are presented in Table 3.

**Explanation Refinement** We instruct gpt-4o to generate explanations, use spacy for phrase segmentation, and refine for 3 iterations. Top-5, Top-10, and Overall Similarity between text phrases and image regions are evaluated to guide refinement, and the top 10 phrases are retained, exemplified in Figure 5. Additionally, Type-Token-Ratio (TTR↑), normalized Shannon Entropy (SE↑) and Perplexity (PPL↓, tokenized using gpt-2) are employed to evaluate lexical diversity, information density and fluency, with results shown in Figure 6. Throughout refinement iterations, all similarity metrics, TTR and SE improved. However, PPL also rose due to the retention of specialized or

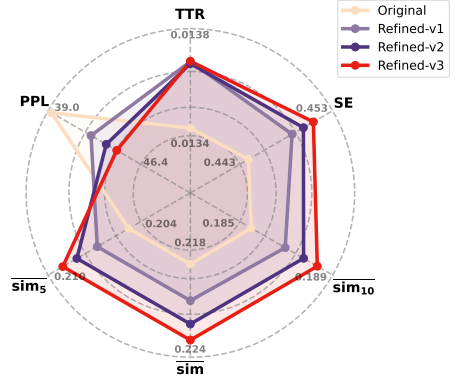


Figure 6. Metrics average across all 8 subsets of GenExplain regarding the initial explanations and their refined versions.

domain-specific terms uncommon in general language usage. Meanwhile, our *Original* setting reflects the effect of baselines directly utilizing MLLMs for explanation, falling short on most metrics.

### 4.3. Robustness Experiments

In real-world scenarios, images awaiting detection often exhibit degradation. Following established procedures [23, 42, 43], and additionally incorporating post-processing operations to better mimic actual cases, we assess the resilience of our method to distribution shifts by introducing three types of perturbations to test images: Gaussian blur ( $\sigma \in [0.5, 2.5]$  pixels), arbitrary rotation ( $\theta \in [-45^\circ, 45^\circ]$ ), and illumination variation (brightness factor  $\alpha \in [0.3, 1.8]$ ). All models are trained on the original unmodified images for evaluation, and the best-performing baselines are compared. As our method is exceptionally trained on more

Method	MJ	SD1.4	SD1.5	ADM	GLI	WK	VQ	BG	Avg.
FreqNet	<b>85.67</b>	84.50	84.94	<b>70.25</b>	77.50	74.25	73.25	76.08	78.31
NPR	65.58	49.92	50.00	57.50	68.75	50.83	68.25	<b>78.17</b>	61.13
DRCT	<b>85.67</b>	81.58	<b>91.08</b>	70.00	78.58	70.92	68.25	73.75	77.48
<b>ESIDE</b>	84.08	<b>86.58</b>	86.06	70.00	<b>85.08</b>	<b>82.08</b>	<b>74.58</b>	76.58	<b>80.63</b>

Table 4. Robustness performance evaluated on perturbed test subsets of GenImage. Subset names are abbreviated.

Setting	DDIM	$\alpha_k$	$w_{k,i}$	Acc (%)	$\Delta$
<b>ESIDE</b>	✓	✓	✓	<b>94.98</b> /99.00	0.00/0.00
– DDIM-Interm.	✓	✓	✓	94.37/98.00	-0.61/-1.00
– DDIM	✗	✓	✓	89.27/99.00	-5.71/0.00
– $\alpha_k$	✗	✗	✓	88.75/98.92	-6.23/-0.08
– $\alpha_k, w_{k,i}$	✗	✗	✗	88.53/ <b>99.17</b>	-6.45/0.17

Table 5. Ablation studies of architectural components on detection results. Models are trained on GenImage/GLIDE.

challenging samples, superior robustness is demonstrated, as observed in Table 4.

#### 4.4. Ablation Studies

**Noised Images and Ensembling** Would simply using unnoised or fully noised images perform better, and is performance increase merely due to the ensembling strategy? To test this hypothesis, we evaluated four different settings correspondingly replacing partially-noised images of intermediate steps with fully-noised images, ensembling on unnoised images, removing ensembling, and eliminating misclassification-centric training. Table 5 shows that our method achieves an accuracy increase of 5.71% on hard samples compared to ensembling entirely on unnoised images, while deactivating model weights and sample weights further decreases performance. Ensembling a model trained on unnoised images with multiple models trained on fully noised images degrades performance on both distributions, implying that features from varying timesteps are utilized.

**High-Frequency Peaks Utilization** For both synthetic and natural images, we suppressed the highest percentile of their Fourier frequencies to a fixed ratio, while masking the commonly-shared components located within a specific bandwidth along the axes, and then used images reconstructed based on these modified spectra for training and evaluation. Table 7 supports our insight that these frequency peaks could be captured by intermediate-step detectors to enhance detection capability regarding more questionable instances, as their suppression halves ensemble effect.

Bandwidth	Suppression	Percentile	Acc (%)	$\Delta$
0.06	0.1	0.15	92.52/98.83	-2.46/-0.17
0.08	0.2	0.10	92.74/98.92	-2.24/-0.08

Table 6. Effects of suppressing high-frequency peaks of Fourier power spectra quadrants. Models are trained and evaluated on reconstructions of GenImage/GLIDE.

## 5. Conclusion

We present ESIDE, a novel pipeline for detecting and explaining synthetic images. We train an ensemble on noised images to directly utilize intermediate features introduced through DDIM inversion, circumventing conventional reconstruction measures. To improve human perception of fake images, we introduce an explanation generation and refinement module. Additionally, we construct two datasets, GenHard and GenExplain, comprising more challenging samples and providing categorized flaw types with explanations for AI-generated images. Extensive experiments show state-of-the-art performance on both regular and harder images, with significant improvements on tougher samples. Our method also generalizes effectively, demonstrates robustness, and enables hybrid parallelism easily.

## Limitations

Our detection method circumvents conventional diffusion reconstruction, but still utilizes partially noised images that requires a rather time-consuming preceding DDIM inversion process. While our simple discriminator architecture enables faster training than existing detectors, the need to train multiple models for an ensemble cannot be denied, though being significantly less time-costing than DDIM inversion. Additionally, as we rely on MLLMs in our explanation and refinement process, explanation quality remains dependent on instruction-prompted MLLM performance. Throughout refining the GENEXPLAIN dataset, 5 out of 6 quality metrics improved on average. However, it can not be guaranteed for each individual case that the MLLM performs effectively and generates higher-rated explanations, leading to rare loss of refinement effectiveness.

## Societal Impacts

Advances in diffusion models and AI-generated content have enabled the creation of deceptively real images, delighting users while simultaneously raising significant ethical concerns. Our study offers a novel solution to the rapidly evolving landscape of synthetic image detection, aiming to address the societal challenges posed by the malicious use of AI-generated images and mitigate potential security risks associated with their proliferation. We employ gpt-4o to

generate explanations for synthetic images, which may occasionally produce uncontrollable generated content requiring further discrimination. Another point to note is that our GENHARD and GENEXPLAIN datasets use images from the GenImage benchmark, which may include disturbing images with diffusion-generated malformed content, particularly in images regarding human faces or animals.

## References

- [1] James Betker, Gabriel Goh, Li Jing, Tim Brooks, Jianfeng Wang, Linjie Li, Long Ouyang, Juntang Zhuang, Joyce Lee, Yufei Guo, et al. Improving image generation with better captions. *Computer Science*. <https://cdn.openai.com/papers/dall-e-3.pdf>, 2(3):8, 2023. 1, 3
- [2] Andrew Brock, Jeff Donahue, and Karen Simonyan. Large scale gan training for high fidelity natural image synthesis. In *International Conference on Learning Representations*, 2019. 5
- [3] Baoying Chen, Jishen Zeng, Jianquan Yang, and Rui Yang. Drct: Diffusion reconstruction contrastive training towards universal detection of diffusion generated images. In *Forty-first International Conference on Machine Learning*, 2024. 1, 3, 6, 11
- [4] Jiaxuan Chen, Jieteng Yao, and Li Niu. A single simple patch is all you need for ai-generated image detection. *arXiv preprint arXiv:2402.01123*, 2024. 3
- [5] Riccardo Corvi, Davide Cozzolino, Giovanni Poggi, Koki Nagano, and Luisa Verdoliva. Intriguing properties of synthetic images: from generative adversarial networks to diffusion models. In *Proceedings of the IEEE/CVF conference on computer vision and pattern recognition*, pages 973–982, 2023. 1, 3
- [6] Davide Cozzolino, Giovanni Poggi, Riccardo Corvi, Matthias Nießner, and Luisa Verdoliva. Raising the bar of ai-generated image detection with clip. In *Proceedings of the IEEE/CVF Conference on Computer Vision and Pattern Recognition*, pages 4356–4366, 2024. 1, 3, 5, 6, 11
- [7] Prafulla Dhariwal and Alexander Nichol. Diffusion models beat gans on image synthesis. *Advances in neural information processing systems*, 34:8780–8794, 2021. 5
- [8] Tarik Dzanic, Karan Shah, and Freddie Witherden. Fourier spectrum discrepancies in deep network generated images. *Advances in neural information processing systems*, 33: 3022–3032, 2020. 1, 3
- [9] Yoav Freund and Robert E Schapire. A decision-theoretic generalization of on-line learning and an application to boosting. *Journal of computer and system sciences*, 55(1): 119–139, 1997. 4
- [10] Shuyang Gu, Dong Chen, Jianmin Bao, Fang Wen, Bo Zhang, Dongdong Chen, Lu Yuan, and Baining Guo. Vector quantized diffusion model for text-to-image synthesis. *2022 IEEE/CVF Conference on Computer Vision and Pattern Recognition (CVPR)*, pages 10686–10696, 2021. 5
- [11] Kaiming He, X. Zhang, Shaoqing Ren, and Jian Sun. Deep residual learning for image recognition. *2016 IEEE Conference on Computer Vision and Pattern Recognition (CVPR)*, pages 770–778, 2015. 6, 11
- [12] Zhengchao Huang, Bin Xia, Zicheng Lin, Zhun Mou, Wenming Yang, and Jiaya Jia. Ffaa: Multimodal large language model based explainable open-world face forgery analysis assistant. *arXiv preprint arXiv:2408.10072*, 2024. 3
- [13] Hengrui Kang, Siwei Wen, Zichen Wen, Junyan Ye, Weijia Li, Peilin Feng, Baichuan Zhou, Bin Wang, Dahua Lin, Linfeng Zhang, et al. Legion: Learning to ground and explain for synthetic image detection. *arXiv preprint arXiv:2503.15264*, 2025. 3
- [14] Linda Laurier, Ave Giulietta, Arlo Octavia, and Meade Cleti. The cat and mouse game: The ongoing arms race between diffusion models and detection methods. *arXiv preprint arXiv:2410.18866*, 2024. 3
- [15] Kuang-Huei Lee, Xi Chen, Gang Hua, Houdong Hu, and Xiaodong He. Stacked cross attention for image-text matching. In *Proceedings of the European conference on computer vision (ECCV)*, pages 201–216, 2018. 4
- [16] Mingxiao Li, Tingyu Qu, Ruicong Yao, Wei Sun, and Marie-Francine Moens. Alleviating exposure bias in diffusion models through sampling with shifted time steps. *arXiv preprint arXiv:2305.15583*, 2023. 2
- [17] Yixuan Li, Xuelin Liu, Xiaoyang Wang, Bu Sung Lee, Shiqi Wang, Anderson Rocha, and Weisi Lin. Fakebench: Probing explainable fake image detection via large multimodal models. *arXiv preprint arXiv:2404.13306*, 2024. 3, 5
- [18] Li Lin, Irene Amerini, Xin Wang, Shu Hu, et al. Robust clip-based detector for exposing diffusion model-generated images. In *2024 IEEE International Conference on Advanced Video and Signal Based Surveillance (AVSS)*, pages 1–7. IEEE, 2024. 3
- [19] Bo Liu, Fan Yang, Xiuli Bi, Bin Xiao, Weisheng Li, and Xinbo Gao. Detecting generated images by real images. In *European Conference on Computer Vision*, pages 95–110. Springer, 2022. 1, 3
- [20] Haotian Liu, Chunyuan Li, Qingyang Wu, and Yong Jae Lee. Visual instruction tuning. *Advances in neural information processing systems*, 36:34892–34916, 2023. 3
- [21] Yang Liu, Xiaofei Li, Jun Zhang, Shengze Hu, and Jun Lei. Da-hfnet: Progressive fine-grained forgery image detection and localization based on dual attention. In *2024 3rd International Conference on Image Processing and Media Computing (ICIPMC)*, pages 51–58. IEEE, 2024. 3
- [22] Ze Liu, Yutong Lin, Yue Cao, Han Hu, Yixuan Wei, Zheng Zhang, Stephen Lin, and Baining Guo. Swin transformer: Hierarchical vision transformer using shifted windows. *2021 IEEE/CVF International Conference on Computer Vision (ICCV)*, pages 9992–10002, 2021. 6, 11
- [23] Peter Lorenz, Ricard L Durall, and Janis Keuper. Detecting images generated by deep diffusion models using their local intrinsic dimensionality. In *Proceedings of the IEEE/CVF International Conference on Computer Vision*, pages 448–459, 2023. 7
- [24] Yunpeng Luo, Junlong Du, Ke Yan, and Shouhong Ding. Lare<sup>2</sup>: Latent reconstruction error based method for diffusion-generated image detection. In *Proceedings of the IEEE/CVF Conference on Computer Vision and Pattern Recognition*, pages 17006–17015, 2024. 1, 3

[25] Ruipeng Ma, Jinhao Duan, Fei Kong, Xiaoshuang Shi, and Kaidi Xu. Exposing the fake: Effective diffusion-generated images detection. *arXiv preprint arXiv:2307.06272*, 2023. 1, 3

[26] Melanie Mathys, Marco Willi, and Raphael Meier. Synthetic photography detection: A visual guidance for identifying synthetic images created by ai. *arXiv preprint arXiv:2408.06398*, 2024. 5

[27] Midjourney, 2022. 1, 3, 5

[28] Alex Nichol, Prafulla Dhariwal, Aditya Ramesh, Pranav Shyam, Pamela Mishkin, Bob McGrew, Ilya Sutskever, and Mark Chen. Glide: Towards photorealistic image generation and editing with text-guided diffusion models. In *International Conference on Machine Learning*, 2021. 5

[29] Utkarsh Ojha, Yuheng Li, and Yong Jae Lee. Towards universal fake image detectors that generalize across generative models. In *Proceedings of the IEEE/CVF Conference on Computer Vision and Pattern Recognition*, pages 24480–24489, 2023. 3, 6, 11

[30] Alec Radford, Jong Wook Kim, Chris Hallacy, Aditya Ramesh, Gabriel Goh, Sandhini Agarwal, Girish Sastry, Amanda Askell, Pamela Mishkin, Jack Clark, Gretchen Krueger, and Ilya Sutskever. Learning transferable visual models from natural language supervision. In *International Conference on Machine Learning*, 2021. 3, 5

[31] B Srinivasa Reddy and Biswanath N Chatterji. An fft-based technique for translation, rotation, and scale-invariant image registration. *IEEE transactions on image processing*, 5(8):1266–1271, 1996. 2

[32] Shaoqing Ren, Kaiming He, Ross Girshick, and Jian Sun. Faster r-cnn: Towards real-time object detection with region proposal networks. *Advances in neural information processing systems*, 28, 2015. 4

[33] Robin Rombach, A. Blattmann, Dominik Lorenz, Patrick Esser, and Björn Ommer. High-resolution image synthesis with latent diffusion models. 2022 *IEEE/CVF Conference on Computer Vision and Pattern Recognition (CVPR)*, pages 10674–10685, 2021. 1, 3, 5

[34] Zeyang Sha, Zheng Li, Ning Yu, and Yang Zhang. De-fake: Detection and attribution of fake images generated by text-to-image generation models. In *Proceedings of the 2023 ACM SIGSAC conference on computer and communications security*, pages 3418–3432, 2023. 1, 3

[35] Jascha Sohl-Dickstein, Eric Weiss, Niru Maheswaranathan, and Surya Ganguli. Deep unsupervised learning using nonequilibrium thermodynamics. In *International conference on machine learning*, pages 2256–2265. pmlr, 2015. 3

[36] Jiaming Song, Chenlin Meng, and Stefano Ermon. Denoising diffusion implicit models. In *International Conference on Learning Representations*, 2021. 2, 4

[37] Jiawei Song, Dengpan Ye, and Yunming Zhang. Trinity detector: text-assisted and attention mechanisms based spectral fusion for diffusion generation image detection. *IEEE Signal Processing Letters*, 2024. 3

[38] Chuangchuang Tan, Yao Zhao, Shikui Wei, Guanghua Gu, and Yunchao Wei. Learning on gradients: Generalized artifacts representation for gan-generated images detection. In *Proceedings of the IEEE/CVF Conference on Computer Vision and Pattern Recognition*, pages 12105–12114, 2023. 1, 3, 6, 11

[39] Chuangchuang Tan, Yao Zhao, Shikui Wei, Guanghua Gu, Ping Liu, and Yunchao Wei. Frequency-aware deepfake detection: Improving generalizability through frequency space domain learning. In *Proceedings of the AAAI Conference on Artificial Intelligence*, pages 5052–5060, 2024. 3, 6, 11

[40] Chuangchuang Tan, Yao Zhao, Shikui Wei, Guanghua Gu, Ping Liu, and Yunchao Wei. Rethinking the up-sampling operations in cnn-based generative network for generalizable deepfake detection. In *Proceedings of the IEEE/CVF Conference on Computer Vision and Pattern Recognition*, pages 28130–28139, 2024. 3, 6, 11

[41] Hugo Touvron, Matthieu Cord, Matthijs Douze, Francisco Massa, Alexandre Sablayrolles, and Herv'e J'egou. Training data-efficient image transformers & distillation through attention. In *International Conference on Machine Learning*, 2020. 6, 11

[42] Sheng-Yu Wang, Oliver Wang, Richard Zhang, Andrew Owens, and Alexei A. Efros. Cnn-generated images are surprisingly easy to spot... for now. 2020 *IEEE/CVF Conference on Computer Vision and Pattern Recognition (CVPR)*, pages 8692–8701, 2019. 1, 3, 6, 7, 11

[43] Zhendong Wang, Jianmin Bao, Wen gang Zhou, Weilun Wang, Hezhen Hu, Hong Chen, and Houqiang Li. Dire for diffusion-generated image detection. 2023 *IEEE/CVF International Conference on Computer Vision (ICCV)*, pages 22388–22398, 2023. 1, 3, 5, 6, 7, 11

[44] Siwei Wen, Junyan Ye, Peilin Feng, Hengrui Kang, Zichen Wen, Yize Chen, Jiang Wu, Wenjun Wu, Conghui He, and Weijia Li. Spot the fake: Large multimodal model-based synthetic image detection with artifact explanation. *arXiv preprint arXiv:2503.14905*, 2025. 3

[45] Wukong, 2022. 5

[46] Juncong Xu, Yang Yang, Han Fang, Honggu Liu, and Weiming Zhang. Famsec: A few-shot-sample-based general ai-generated image detection method. *IEEE Signal Processing Letters*, 2024. 3

[47] Zhipei Xu, Xuanyu Zhang, Runyi Li, Zecheng Tang, Qing Huang, and Jian Zhang. Fakeshield: Explainable image forgery detection and localization via multi-modal large language models. *ArXiv*, abs/2410.02761, 2024. 3, 5

[48] Junyan Ye, Baichuan Zhou, Zilong Huang, Junan Zhang, Tianyi Bai, Hengrui Kang, Jun He, Honglin Lin, Zihao Wang, Tong Wu, et al. Loki: A comprehensive synthetic data detection benchmark using large multimodal models. *arXiv preprint arXiv:2410.09732*, 2024. 3

[49] Nan Zhong, Yiran Xu, Zhenxing Qian, and Xinpeng Zhang. Rich and poor texture contrast: A simple yet effective approach for ai-generated image detection. *CoRR*, 2023. 1, 3

[50] Mingjian Zhu, Hanting Chen, Qiangyu Yan, Xudong Huang, Guanyu Lin, Wei Li, Zhijun Tu, Hailin Hu, Jie Hu, and Yunhe Wang. Genimage: A million-scale benchmark for detecting ai-generated image. *Advances in Neural Information Processing Systems*, 36:77771–77782, 2023. 5, 11

Bandwidth	Suppression	Percentile	Acc (%)	$\Delta$
0.06	0.1	0.15	92.52/98.83	-2.46/-0.17
0.08	0.2	0.10	92.74/98.92	-2.24/-0.08
0.00	0.2	0.10	93.27/98.17	-1.71/-0.83

Table 7. Effects of suppressing high-frequency peaks of Fourier power spectra quadrants on detection results. Models are trained on reconstructions of GenImage/GLIDE, and all the samples trained and evaluated are reconstructed through modified Fourier power spectra.

## A. Experimental Details

Further experimental settings, ablation studies, hyperparameter details, result analysis and questionable aspects are described and resolved in the sections below.

### A.1. Fourier Power Spectra Analysis

For both synthetic and natural images, we suppress Fourier frequencies with the highest percentile of energy levels of the spectra to a small ratio of their original energy levels. We applied a mask of a specific bandwidth radius along the main horizontal and vertical axes by proportion of image width and height. Frequencies within this bandwidth are not recorded or suppressed, as both synthetic and natural images show high frequencies in these regions, which may obscure actual intriguing peaks. Synthetic and natural images were then reconstructed based on these modified spectra, and used for training and evaluation. An example of this process is depicted in Figure 7, while quantitative histograms of the energy levels of synthetic and natural images from varying diffusion timesteps are depicted in Figure 8.

Experimental results in Table 7 shows accuracy drops on challenging samples that approximate half of not ensembling at all, while accuracies remain nearly the same on original samples. This supports our hypothesis that these previously inapparent high-frequency peaks revealed through diffusion noising could be captured by intermediate-step detectors to enhance detection quality on more questionable instances. Meanwhile, not applying a masked bandwidth when suppressing frequencies results in the loss of image characteristics, and decreases accuracy on original samples.

### A.2. Synthetic Image Detection

**MLLM Detection** With the proliferation of large multi-modal models, an intuitive idea would be to conduct the entire detection process with MLLMs. However, as shown in Table 8, these models currently fail to achieve comparable performance with specialized detection methods, refuse to predict when facing confusing scenarios, while synthetic images may be blocked from use occasionally.

Predictions	Label: Synthetic	Label: Natural
Synthetic	86.95	9.50
Natural	6.78	84.05
Refuse to Answer	6.13	6.45
Policy Issues	0.13	0.00

Table 8. Synthetic image detection prediction distributions of gpt-4o on GenImage/GLIDE original samples. Accuracies are significantly lower than current detection baselines.

Method	Flux	GenImage Avg.
CBSID	73.64/99.42	81.64/95.95
FreqNet	77.70/89.33	91.22/94.82
NPR	92.23/98.67	92.43/95.85
DRCT	84.46/98.17	93.19/98.36
<b>ESIDE</b>	<b>94.26/99.58</b>	<b>95.89/98.91</b>

Table 9. Synthetic image detection accuracies on Flux.

Architecture	ESIDE	CBSID
Net-XS	89.79/98.75	74.03/99.25
Net-S	92.22/98.67	86.86/ <b>99.33</b>
Net-M	<b>94.42/99.33</b>	87.93/99.08
<b>Net-L</b>	<b>94.98/99.00</b>	88.53/99.17
Net-XL	93.56/98.42	86.92/99.25
Net-LW	93.34/98.50	86.12/ <b>99.33</b>

Table 10. Comparison of effects of discriminator architectures. Models are trained on GenImage/GLIDE.

**Flux-generated images** Flux is an emerging generative model capable of producing high-quality images. To test our method’s performance when facing images from such generators, we generated 12,000 synthetic images with FLUX.1-dev, paired with natural images of the same item classes, and tested our method with the top-performing baselines on the harder and original images generated. Our method also demonstrates state-of-the-art performance when detecting synthetic images from up-to-date generators like Flux, and leads in performance even more than on GenImage [50] as compared to baselines.

**Baseline Settings** For ResNet-50 [11], we initialized our model with the weights pre-trained on ImageNet, then fine-tuned it on our synthetic image detection task. For CBSID [6], we reimplemented it using the same classifier architecture as ours. For DeiT-S [41], Swin-T [22], CNNSpot [42], CBSID , DIRE [43], LGrad [38], UnivFD [29], FreqNet [39], NPR [40], and DRCT [3], we utilized the officially provided implementations from their GitHub repositories to conduct model training and evaluation.

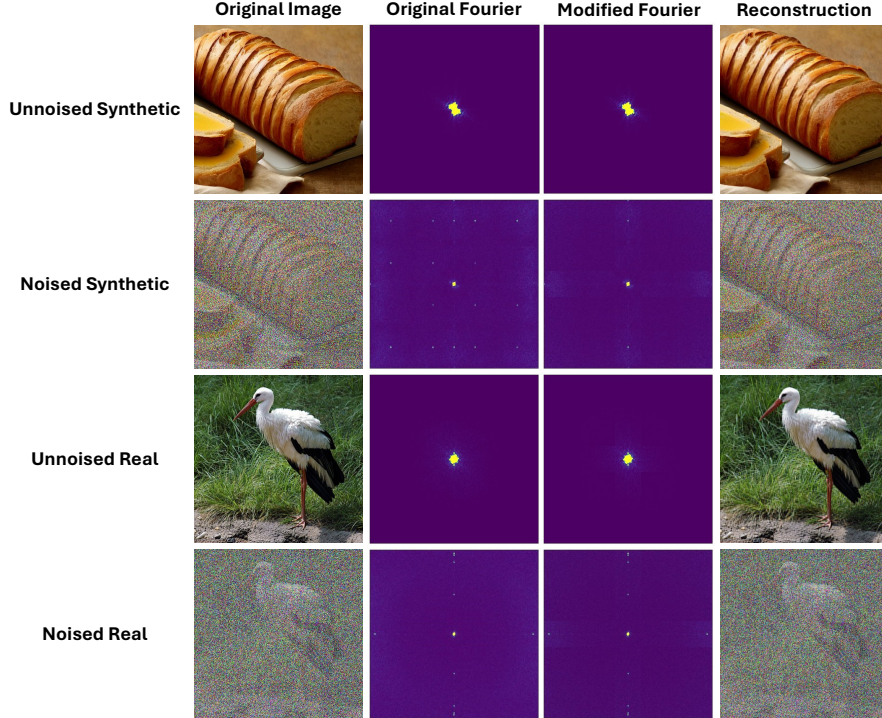


Figure 7. Fourier power spectra of synthetic and real images at timestep 0 and 12 of a 24-timestep DDIM inversion process. Energy levels of high-frequency peaks in the quadrants of the spectra are suppressed, and images are reconstructed based on these modified spectra and used for detection ablations. Synthetic images show prominent peaks in the quadrants, while real images show smooth and circular decrements.

**Classifier Architecture** We evaluated linear network layers of varying depths and dimensions for our classifiers, to find an optimal design that balances efficiency and performance. We compared our results with the CBSID baseline of the same architecture, as shown in Table 10. Each network has an input size of 768 and a scalar output, with hidden layer sizes listed below. Of all the architectures tested, Net-L performs best overall in terms of accuracy, and is used for all of our other experiments.

- **Net-XS:** 256
- **Net-S:** 512, 256
- **Net-M:** 512, 256, 128
- **Net-L:** 1024, 512, 256, 128
- **Net-XL:** 1024, 1024, 512, 256, 128
- **Net-LW:** 2048, 1024, 512, 256

**Diffusion Timestep Stride** The amount of models in the ensemble greatly affects training, to determine what timestep stride is the best for balancing performance and efficiency, we experimented with numerous ensemble sizes, as depicted in Table 11. Notably, optimal performance is attained when employing a stride size of 3 instead of a unit stride. Classifiers trained on the original images typ-

Test Split	$s = 1$	$s = 2$	$s = 3$	$s = 4$	$s = 6$	$s = 8$	$s = 12$
Hard	93.30	93.53	<b>94.98</b>	93.21	92.95	93.94	91.77
Original	98.58	98.42	<b>99.00</b>	98.33	98.33	98.75	98.42

Table 11. Comparison of diffusion timestep strides on detection results. Models are trained on GenImage/GLIDE.

Timestep	0	3	6	9	12	15	18	21	24
Acc	<b>99.25</b>	93.42	93.00	93.33	94.48	96.17	96.50	96.75	96.42

Table 12. Performance of 9 CBSID classification models on original samples, individually trained on noised images from different diffusion timesteps. Models are trained on GenImage/GLIDE, Net-XS architecture.

ically have higher accuracy and are assigned larger model weights, as shown in Table 12. Ensembling too many noised classifiers tend to outweigh and neglect the original, thus slightly lowering accuracy. Nevertheless, when facing controversial samples, utilizing latent features enables them to coordinate overturn the unnoised discriminator’s erroneous judgment, enhancing overall accuracy.

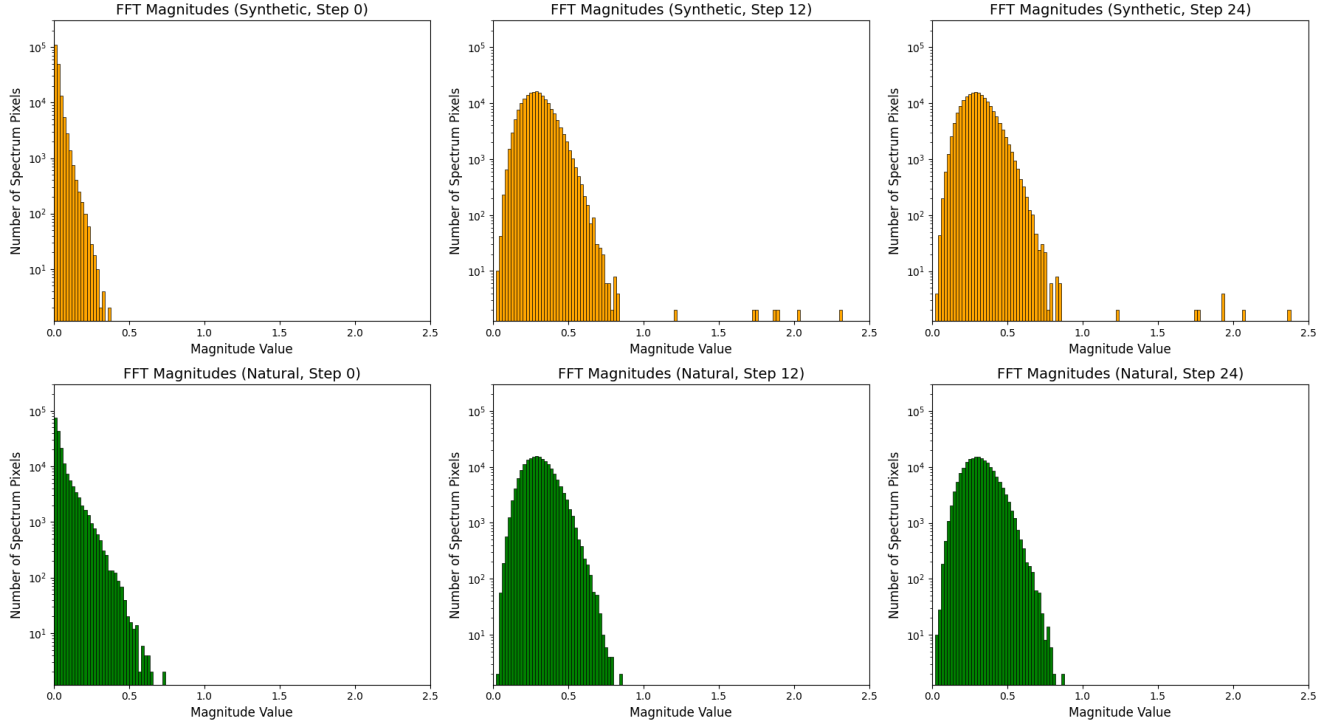


Figure 8. Energy magnitude histograms of Fourier power spectra of synthetic and real images at timestep 0, 12 and 24 of a 24-timestep DDIM inversion process. A bandwidth along the axes is masked. Synthetic images show high-frequency peaks gradually amplified by noising, unobserved in real images.

Metric	Original	Refined-v1	Refined-v2	Refined-v3
$\overline{sim}_5$ ( $\uparrow$ )	0.2192	0.2211	0.2223	<b>0.2232</b>
$\overline{sim}_{10}$ ( $\uparrow$ )	0.2046	0.2067	0.2081	<b>0.2091</b>
$\overline{sim}$ ( $\uparrow$ )	0.1859	0.1871	0.1877	<b>0.1882</b>
TTR ( $\uparrow$ )	0.01344	<b>0.01369</b>	0.01368	<b>0.01369</b>
SE ( $\uparrow$ )	0.4443	0.4487	0.4499	<b>0.4509</b>
PPL ( $\downarrow$ )	<b>39.32</b>	42.45	43.66	44.49

Table 13. Evaluation metrics average of each iteration during the explanation refinement process on GenExplain.

### A.3. Error Explanation

**Flaw Classification** For flaw classification, a predicted label is considered “True” if the model’s output logit is greater than or equal to 0.5 and “False” otherwise. The predictions for each flaw label are computed independently.

**Explanation Refinement** Evaluation metric averages during explanation refinement are provided in Table 13, while detailed values on each subset are provided in Table 14 to Table 21. Monotonic increases in similarity, TTR and SE indicate that refined explanations have higher relevance with the original image, and possess higher lexical di-

Metric	Original	Refined-v1	Refined-v2	Refined-v3
$\overline{sim}_5$ ( $\uparrow$ )	0.2206	0.2226	0.2241	<b>0.2249</b>
$\overline{sim}_{10}$ ( $\uparrow$ )	0.2035	0.2057	0.2073	<b>0.2082</b>
$\overline{sim}$ ( $\uparrow$ )	0.1824	0.1837	0.1845	<b>0.1850</b>
TTR ( $\uparrow$ )	0.01882	0.01919	0.01930	<b>0.01932</b>
SE ( $\uparrow$ )	0.4625	0.4679	0.4688	<b>0.4697</b>
PPL ( $\downarrow$ )	<b>38.18</b>	41.52	42.44	43.29

Table 14. Evaluation metrics of each iteration during the explanation refinement process on GenExplain/Midjourney.

versity and information density. However, increases in PPL indicate that refining decreases fluency, attributed to the retention of specialized or domain-specific terms uncommon in general language usage.

Metric	Original	Refined-v1	Refined-v2	Refined-v3
$\overline{sim}_5$ ( $\uparrow$ )	0.2190	0.2212	0.2226	<b>0.2237</b>
$\overline{sim}_{10}$ ( $\uparrow$ )	0.2025	0.2049	0.2063	<b>0.2075</b>
$\overline{sim}$ ( $\uparrow$ )	0.1824	0.1837	0.1844	<b>0.1849</b>
TTR ( $\uparrow$ )	0.01226	0.01250	<b>0.01251</b>	<b>0.01251</b>
SE ( $\uparrow$ )	0.4410	0.4452	0.4462	<b>0.4473</b>
PPL ( $\downarrow$ )	<b>39.23</b>	42.13	43.25	44.08

Table 15. Evaluation metrics of each iteration during the explanation refinement process on GenExplain/SD V1.4.

Metric	Original	Refined-v1	Refined-v2	Refined-v3
$\overline{sim}_5$ ( $\uparrow$ )	0.2217	0.2239	0.2253	<b>0.2261</b>
$\overline{sim}_{10}$ ( $\uparrow$ )	0.2050	0.2074	0.2089	<b>0.2099</b>
$\overline{sim}$ ( $\uparrow$ )	0.1845	0.1858	0.1865	<b>0.1870</b>
TTR ( $\uparrow$ )	0.01951	0.01990	0.01992	<b>0.01995</b>
SE ( $\uparrow$ )	0.4637	0.4684	0.4701	<b>0.4712</b>
PPL ( $\downarrow$ )	<b>40.32</b>	43.55	44.84	45.58

Table 16. Evaluation metrics of each iteration during the explanation refinement process on GenExplain/SD V1.5.

Metric	Original	Refined-v1	Refined-v2	Refined-v3
$\overline{sim}_5$ ( $\uparrow$ )	0.2181	0.2197	0.2207	<b>0.2213</b>
$\overline{sim}_{10}$ ( $\uparrow$ )	0.2057	0.2075	0.2087	<b>0.2094</b>
$\overline{sim}$ ( $\uparrow$ )	0.1890	0.1899	0.1904	<b>0.1908</b>
TTR ( $\uparrow$ )	0.01272	<b>0.01280</b>	0.01277	0.01273
SE ( $\uparrow$ )	0.4420	0.4458	0.4468	<b>0.4479</b>
PPL ( $\downarrow$ )	<b>39.78</b>	42.67	43.74	44.81

Table 17. Evaluation metrics of each iteration during the explanation refinement process on GenExplain/ADM.

Metric	Original	Refined-v1	Refined-v2	Refined-v3
$\overline{sim}_5$ ( $\uparrow$ )	0.2233	0.2253	0.2265	<b>0.2275</b>
$\overline{sim}_{10}$ ( $\uparrow$ )	0.2087	0.2109	0.2123	<b>0.2133</b>
$\overline{sim}$ ( $\uparrow$ )	0.1900	0.1912	0.1918	<b>0.1923</b>
TTR ( $\uparrow$ )	0.01064	<b>0.01085</b>	0.01074	0.01072
SE ( $\uparrow$ )	0.4334	0.4380	0.4390	<b>0.4400</b>
PPL ( $\downarrow$ )	<b>38.50</b>	41.31	42.40	43.12

Table 18. Evaluation metrics of each iteration during the explanation refinement process on GenExplain/GLIDE.

Metric	Original	Refined-v1	Refined-v2	Refined-v3
$\overline{sim}_5$ ( $\uparrow$ )	0.2203	0.2226	0.2239	<b>0.2248</b>
$\overline{sim}_{10}$ ( $\uparrow$ )	0.2052	0.2075	0.2090	<b>0.2100</b>
$\overline{sim}$ ( $\uparrow$ )	0.1861	0.1873	0.1879	<b>0.1885</b>
TTR ( $\uparrow$ )	0.01227	0.01239	0.01239	<b>0.01245</b>
SE ( $\uparrow$ )	0.4420	0.4453	0.4465	<b>0.4477</b>
PPL ( $\downarrow$ )	<b>40.11</b>	43.05	44.26	45.08

Table 19. Evaluation metrics of each iteration during the explanation refinement process on GenExplain/Wukong.

Metric	Original	Refined-v1	Refined-v2	Refined-v3
$\overline{sim}_5$ ( $\uparrow$ )	0.2161	0.2177	0.2187	<b>0.2195</b>
$\overline{sim}_{10}$ ( $\uparrow$ )	0.2036	0.2053	0.2065	<b>0.2074</b>
$\overline{sim}$ ( $\uparrow$ )	0.1856	0.1867	0.1872	<b>0.1876</b>
TTR ( $\uparrow$ )	0.01050	<b>0.01077</b>	0.01075	0.01076
SE ( $\uparrow$ )	0.4341	0.4389	0.4401	<b>0.4410</b>
PPL ( $\downarrow$ )	<b>39.40</b>	42.92	44.37	45.17

Table 20. Evaluation metrics of each iteration during the explanation refinement process on GenExplain/VQDM.

Metric	Original	Refined-v1	Refined-v2	Refined-v3
$\overline{sim}_5$ ( $\uparrow$ )	0.2142	0.2158	0.2169	<b>0.2177</b>
$\overline{sim}_{10}$ ( $\uparrow$ )	0.2028	0.2047	0.2059	<b>0.2068</b>
$\overline{sim}$ ( $\uparrow$ )	0.1870	0.1881	0.1888	<b>0.1892</b>
TTR ( $\uparrow$ )	0.01083	<b>0.01109</b>	0.01105	0.01106
SE ( $\uparrow$ )	0.4360	0.4402	0.4413	<b>0.4420</b>
PPL ( $\downarrow$ )	<b>39.04</b>	42.47	43.98	44.80

Table 21. Evaluation metrics of each iteration during the explanation refinement process on GenExplain/BigGAN.

## B. Prompt Design

### B.1. Flaw Classification Prompt

To generate the initial set of classified image flaws for constructing our GENEXPLAIN dataset, and then train a flaw classification model, we first prompted GPT-4○ to classify these flaws, which were manually filtered afterwards.

#### Flaw Classification Guidelines for Synthetic Images

You will be provided with an AI generated image, try to identify systematic errors that make it distinguishable from natural real images from the categories below:

- 1. Lighting:** Unnatural or inconsistent light sources and shadows.
- 2. Color Saturation or Contrast:** Overly bright or dull colors, extreme contrasts disrupting image harmony.
- 3. Perspective:** Spatial disorientation caused by unrealistic angles or viewpoints, otherwise dimensionality errors such as flattened 3D objects.
- 4. Bad Anatomy:** For living creatures, mismatches and errors of body parts in humans or animals.
- 5. Distorted Objects:** For nonliving objects only, warped objects with fallacious details deviating from expected forms.
- 6. Structural Composition:** Poor positional arrangement between multiple elements in the scene.
- 7. Incomprehensible Text:** Malformed and unrecognizable text.
- 8. Implausible Scenarios:** Inappropriate behavior and situations unlikely to happen based on sociocultural concerns, or contradicting to historical facts.
- 9. Physical Law Violations:** Improbable physics, such as erroneous reflections or objects defying gravity.

Only select the categories below when highly confident:

- 10. Blurry or Inconsistent Borders:** Unclear or abrupt border outlines between elements.
- 11. Background:** Poorly blended or monotonous drab backgrounds.
- 12. Texture:** For nonliving objects only, significantly over-polished or unnatural textural appearances.
- 13. Generation Failures:** Major prominent rendering glitches or incomplete objects disrupting the entire scene.

If NONE of the categories above match, select:

#### 14. Not Evident

Choose one or more categories above, and only reply the indexes of identified errors separated with commas, e.g. "1,3,6" for an image with "Lighting, Perspective, Structural Composition" errors, with no additional explanation.

PLEASE NOTE: Responses MUST be in the format of "[Number 1],[Number 2],..." (numbers and commas only) ordered from low to high, or "14" if no evident errors are found.

## B.2. Initial Explanation Generation Prompt

After manually removing images with flaws that were incorrectly categorized, we prompted GPT-4o-mini to generate an initial explanation based on the description of the identified flaw.

### Initial Explanation Generation Guidelines

You will be provided with an AI generated image confirmed with the following systematic error: <DESCRIPTION OF ERROR CATEGORY>

Give an explanation for why such an error is found in the image, and point out the specific location or items causing the error. Pay close attention to image details.

PLEASE NOTE: Responses should be concise, and organized into a SINGLE PARAGRAPH.

## B.3. Iterative Explanation Refinement Prompt

For 3 rounds we iteratively refined the initial explanation and follow-ups. During each iteration, we calculated the Top-10 similar noun phrases with the synthetic image, and prompted GPT-4o-mini to retain these relevant phrases while additionally searching for overlooked flaws. The final refined explanations were added to our dataset.

### Iterative Explanation Refinement Guidelines

You will be provided with an AI generated image confirmed with <ERROR CATEGORY> error. Below is an explanation of why this error appears in the image: <PREVIOUS EXPLANATION>

In this explanation, the following words may be highly relevant and accurately describe the image: <TOP 10 SIMILARITY PHRASES>

Your task is to refine the explanation to better align with the error in the image while retaining the relevant words. You can also analyze the image to identify whether any other potential errors that may have been overlooked about <ERROR CATEGORY>. Keep the explanation concise and avoid redundancy.

PLEASE NOTE: Responses should be concise, and organized into a SINGLE PARAGRAPH.